Journal Pre-proof

A numerical framework for determination of stress concentration factor distributions in tubular joints

K. Hectors, W. De Waele

PII: S0020-7403(19)33540-4
DOI: https://doi.org/10.1016/j.ijmecsci.2020.105511
Reference: MS 105511

To appear in: *International Journal of Mechanical Sciences*

Received date: 18 September 2019
Revised date: 24 January 2020
Accepted date: 3 February 2020

Please cite this article as: K. Hectors, W. De Waele, A numerical framework for determination of stress concentration factor distributions in tubular joints, *International Journal of Mechanical Sciences* (2020), doi: https://doi.org/10.1016/j.ijmecsci.2020.105511

Highlights

A numerical framework for determination of stress concentration factor distributions in tubular joints

K. Hectors, W. De Waele

- Framework for calculation of hot spot stress distributions in tubular joints.
- The developed framework accurately predicts SCF distributions.
- It was validated to experimental data and parametric equations from literature.
- Including weld geometry can significantly influence SCF calculations.

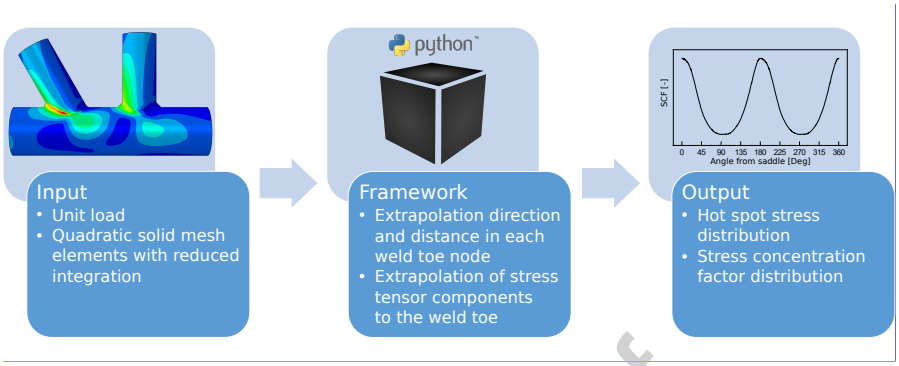

A numerical framework for determination of stress concentration factor distributions in tubular joints

K. Hectors[a,b,*], W. De Waele[a]

[a] *Ghent University, Faculty of Engineering and Architecture, Department of EEMeCS, Laboratory Soete, Belgium*
[b] *SIM vzw, Technologiepark 48, 9052 Zwijnaarde, Belgium*

Abstract

Fatigue design of welded tubular joints implies the calculation of stress concentration factors at distinct weld toe locations using parametric formulas for basic loading cases. A Python based framework for automated calculation of hot spot stress and stress concentration factor distributions along the entire weld is presented. Hot spot stresses are calculated based on extrapolation of surface stresses extracted from a finite element analysis output database. For each node of the weld toes, the extrapolation direction and location dependent distances are first determined. Next the complete stress tensor in each read-out point is extrapolated towards the weld toe. The hot spot stress is determined as the maximum value of three critical stress values following the guidelines of DNV.

A validation study is carried out in which the framework results are compared to both experimental data and parametric equations from literature for three different load cases: axial loading, in-plane bending and out-of-

*Corresponding author
Email address: Kris.Hectors@UGent.be (K. Hectors)

plane bending. The results obtained from the developed framework show good agreement with the experimental results and capture the shape of the stress concentration factor distribution much better than reference parametric equations. Finally, the framework is used to demonstrate the importance of including the weld geometry in the finite element model of the tubular joint. The results show that using a model without a weld can result in overly conservative estimations of stress concentration factors.

Keywords: Tubular joint; Structural stress; Hot-spot stress; Finite element method; Stress analysis

1. Introduction

The Flemish research project SafeLife focuses on lifetime assessment of dynamically loaded industrial structures based on load and condition monitoring. Such an assessment is essential towards decision support for quantification of lifetime extension and optimization of predictive maintenance [1]. However lifetime prediction of welded steel structures, in particular those that are subjected to multi-axial, non-proportional and variable amplitude loading, is known to be extremely complex [2]. Due to developments in numerical modelling methods and the increasing demand for high performance structures and components, design engineers are increasingly using finite element software for fatigue assessment of structural details. Conventional fatigue design is based on the so-called endurance approach where the nominal stress is calculated and subsequently combined with an S-N curve to determine the fatigue life. The chosen S-N curve is based on the classification of the weld detail as defined in standards or guidelines (e.g. Eurocode3

[3], IIW [4]). This design method has two main disadvantages. First, dimensional variations are largely ignored, except for the plate thickness which is accounted for using safety factors. Secondly, complex geometries can often not be classified in the detail categories defined by standards. In order to overcome these disadvantages, the hot spot stress method was developed [5].

The hot spot stress method is used extensively in the assessment of welded offshore structures such as jacket structures used for supporting offshore wind turbines [6]. Offshore jacket structures are manufactured as welded connections between circular hollow sections, this is illustrated in Fig. 1. Large stress concentrations occur at the weld toes which are quantified using a dimensionless stress concentration factor (SCF). The SCF is defined as the ratio of the hot spot stress in a point of the weld toe to the nominal stress in the brace [7]. The SCFs mainly depend on the joint type (e.g. T, Y, K), its dimensions and the loading case. Accurate knowledge of the SCFs is of major importance in fatigue design of tubular joints. The SCFs are generally determined using parametric equations that were obtained from fitting equations to a large data set of hot spot stress calculations of different joints and loading conditions.

In the next section different methods for determination of the hot spot stress are discussed after which an overview of parametric equations for SCFs is presented and their shortcomings identified. Based on these shortcomings a numerical framework for automated calculation of the hot spot stress and corresponding SCF distribution along the whole weld toe line of a tubular joint is presented. The calculation of the hot spot stresses is based on a post-

processing of a finite element output database. The finite element model is briefly described in section 3. In section 4 the discussion of the developed framework is organized in three subsections. The flowchart in Fig. 2 guides the reader through the subsections. It shows the building blocks of the framework, its relation with the finite element model and how the output can be used as an input for a fatigue assessment. At the end of section 3 and each subsection of section 4, a detailed flowchart is included to give the reader a clear and logical overview of the presented methods. The explanation of the framework is followed by two case studies in section 5. The first case study is intended as a validation of the framework, here SCF distributions calculated using the developed framework are compared to numerical and experimental data from literature. In the second case study a preliminary study on the influence of the weld geometry on the SCF distributions is reported. Finally in section 6 the conclusions are summarized.

2. Literature review

2.1. Hot spot stress

The hot spot stress concept dates back to the 1960s when, among others, Peterson, Manson and Haibach showed that the fatigue strength could be related to a local stress or strain that is measured in front of the weld toe [8]. This means that a local stress value (i.e. the hot spot stress) can be defined such that the effect of the global weld geometry effect on the fatigue strength is considered, whilst ignoring the notch effect caused by the weld toe. The hot spot stress method originated as a way to assess the fatigue strength of tubular joints by using it to determine the SCF at different distinct locations

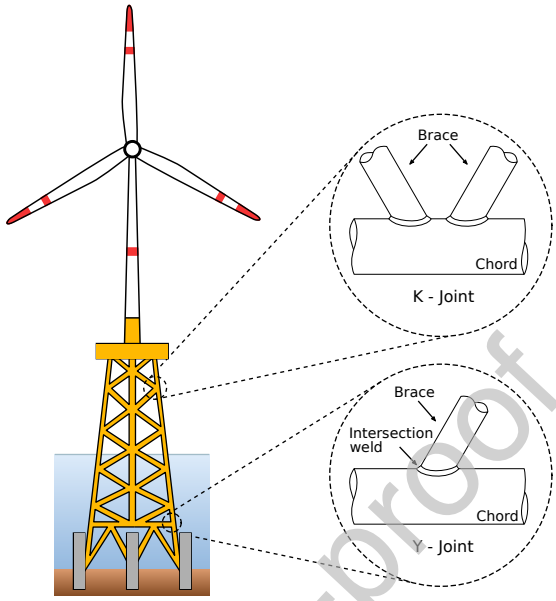

Figure 1: Welded offshore jacket supporting a wind turbine and illustration of two typical configuration of joints between circular hollow sections.

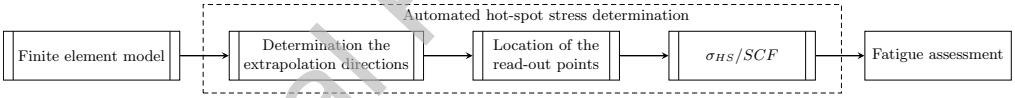

Figure 2: Building blocks of the developed framework

around the weld toe line. The stress used to determine the SCF is referred to as the geometric hot spot stress [3], the structural stress [9] or simply the hot spot stress [10].

Although there is a general agreement as to how the hot spot stress is defined near a weld discontinuity, different methods have been proposed for calculating the hot spot stress [11, 12]. There are three principal methods for determining the hot spot stress: through-thickness stress linearization, the structural stress method and surface stress extrapolation. In the through-

thickness stress linearization method, the hot spot stress is calculated by linearization of the stress through the wall thickness at the weld toe (Fig. 3a) obtained from a finite element analysis. The through-thickness linearization method is especially suitable for relatively thick geometries with a nonlinear stress distribution in front of the weld toe. A disadvantage of the through-thickness linearization is element size dependency of the result. To overcome this Dong, [9, 13] introduced the mesh insensitive structural stress method, which is based on the assumption that the stress concentration at the weld toe can be represented by a stress state that is equivalent to and in equilibrium with the stress state on a section at a distance δ from the weld toe (Fig. 3b). By using balanced nodal forces and moments in the weld toe plane within the context of displacement-based finite element analysis the hot spot stress at the surface can be calculated. Although the method proposed by Dong has been shown to provide accurate, mesh insensitive results for a large number of cases [14, 15], Doerk et al. [11] showed that the mesh insensitivity is lost for complex 3D structures. The meshing outside the stress evaluation area strongly affects the computed stress distribution, which is attributed to the neglect of stresses in the equilibrium equations acting at the transverse element sides [5]. Inspired by the work of Dong, Kim et al. [16] proposed a novel approach to determine the structural stress for welded joints modelled with 3D solid elements. Their approach is based on calculation of the traction stresses acting on cross sections of two imaginary cuts which are parallel to the weld toe and across the base plate. Two different concepts were introduced to calculate the equivalent traction stresses at the weld toe, more specifically force and work equivalence. Compared to Dongs method,

the approach of Kim et al. additionally accounts for an in-plane bending moment while retaining its mesh insensitivity, the difference between the two approaches is illustrated in Fig. 4. Despite this modification, this method is also not capable of accounting for multi-axial stress states since neither the traction stress on the longitudinal surface nor the shear stresses are accounted for. The last method is the surface extrapolation method. In this method, the hot spot stress is obtained by extrapolating the surface stress obtained at two points in front of the weld toe towards the weld toe as illustrated in Fig. 3c. The distance of the reference points relative to each other and relative to the weld toe depends on the design code that is used. In general, the location of the first reference point is defined such that it is located where the nonlinear varying through-thickness stress distribution begins to flatten. The second reference point is located such that the stress increase is captured without being influenced by the global stress concentration [16].

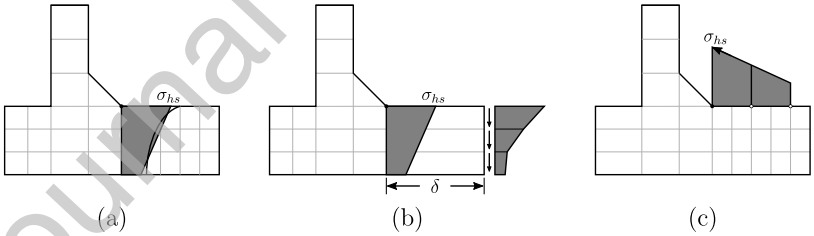

Figure 3: (a) Through-thickness stress linearization method, (b) structural stress method, (c) surface stress extrapolation method

The surface stress extrapolation method is the most common method for determination of the hot spot stresses in tubular joints. This reason for this is associated with the complex geometry and high local bending of the tubular walls [11, 17]. Furthermore, the surface stress extrapolation method can

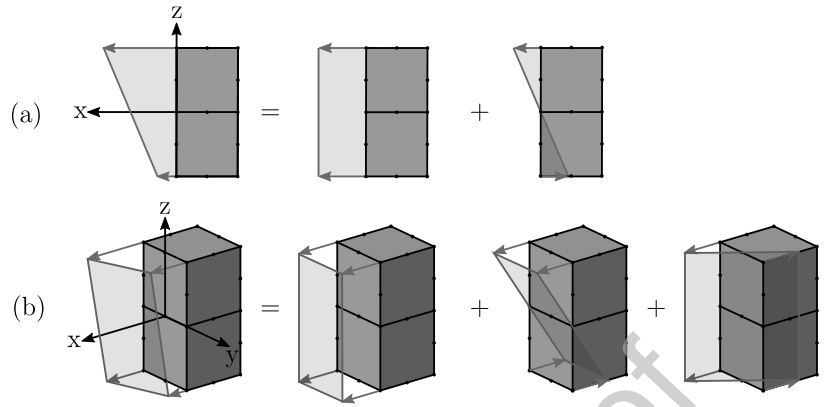

Figure 4: Difference between the structural stress approaches of Dong [13] (a) and Kim et al.[16] (b)

be directly related to experimental measurements with strain gauges placed at the same distance from the weld toe as the reference points used in the numerical models (e.g. [18]). The surface stress extrapolation is recommended most common design codes and standards (e.g DNVGL-RP-C203 [19], CIDECT [20], AWS [21] and API [22]) for (offshore) tubular joints.

Despite the success of the surface stress extrapolation method, the authors want to point out some of its shortcomings. For tubular joints, the two most common ways of determining the hot spot stress with the surface stress extrapolation method are extrapolation of the stress components perpendicular to the weld toe or extrapolation of the maximum principal stresses. The extrapolation of the stress components perpendicular to the weld toe (e.g. [7]) disregards the stress parallel to the weld toe line as well as the shear stress, which could affect the SCF in more complex loading conditions. On the other hand, by calculating the hot spot stress by the extrapolation of the maximal principal stresses at the reference points (e.g [23]) possible dissimilarities of

the orientation of the principal stresses in the extrapolation region are neglected, which contradicts the basic laws of mechanics. The authors are of the opinion that both adaptations of the surface stress extrapolation method should be reconsidered in an effort to obtain the most accurate representation of the stress state at the hot spot.

2.2. Determination of the stress concentration factor for tubular joints

A lot of research towards the development of parametric SCF equations for different tubular joint geometries has been reported. These parametric equations are expressed for three principal modes of loading, i.e. axial loading, in-plane bending (IPB) and out-of-plane bending (OPB), and are generally a function of dimensionless parameters that describe the joint geometry and dimensions. The parametric equations are either based on experimental results or finite element analyses. Examples of parametric equations derived from experiments are the equations of Wordsworth and Smedley (W/S) [24], the UEG (Underwater Engineering Group) equations and the Lloyd's Register (LR) equations [25]. Examples of parametric equations based on finite element analyses are the equations of Kuang [26] that were based on thin-shell models or the Efthymiou equations [27] that were based on thick-shell models. Due to the high costs associated with experiments on representative components, parametric studies using finite element models have become the most used method for deriving SCF parametric equations.

The most widely adopted SCF parametric equations are the Efthymiou equations, originally published in 1985 for T/Y-joints and gap/overlap K joints. They have been adopted by different design codes such as DNV [19] and

CIDECT [20]. Similar to the other sets of parametric equations that were mentioned in the previous paragraph, the Efthymiou equations aim to estimate the SCF at the saddle and crown positions (see Fig. 5), which are assumed to be the most critical locations with respect to failure. This assumption is generally true for the three principal loading modes. However, offshore jackets are subjected to combinations of these three loading modes. This can cause the hot spots, where cracks can initiate, to be located anywhere along the circumference of the intersection between the brace and chord [28]. In order to obtain the SCF in complex loading conditions (i.e. multi-axial loading) superposition of the three principal loading modes is typically performed [19]. However, it has been shown that the use of superposition can result in either an underestimation [29] or an overestimation [30] of the hot spot stress and thus the SCF. Hellier, Connelly and Dover [31] developed a set of equations (the so-called HCD equations) that are similar to the Efthymiou equations but they also developed equations for both angular location and magnitude of the hot spot stress on the circumference of the intersection as they recognized the importance of an accurate knowledge of the failure location [31]. They further complemented this with characteristic formulae for the SCF distribution around the joint circumference. The HCD equations give the characteristics of the stress distribution along the brace/chord intersection and allow the effect of a hot spot at a point other than the crown or saddle to be taken into account. However, they were derived from a limited number of finite element simulations and thus may not be able to capture the effects of all joint sufficiently accurate. Furthermore, the HCD equations that describe the SCF distributions require the

discrete SCFs at the crown and saddle locations as input which themselves are generally determined from other parametric equations [32]. In an effort to overcome these deficiencies, Chang and Dover [32] performed a numerical study for 330 different tubular Y- and T-joints resulting in a different set of parametric SCF equations. However validation of the new equations against experimental results of steel and acrylic joints did not show a significant improvement over the HCD equations.

In 2009, Shao et al. [33] proposed a set of parametric equations to calculate the SCF distributions along the weld toes of K-joints subjected to basic loadings, based on results from extensive parametric finite element analyses. In 2010, Lotfollahi-Yaghin and Ahmadi [34] published their work on the effect of geometrical parameters on the SCF distribution along the weld toe of axially loaded KT-Joints. In 2015 Ahmadi et al. [35] reported the stress distribution around the weld toe on the chord of both an unstiffened and ring-stiffened KT-joint based on strain gauge measurements and finite element simulations. They implemented a macro in the ANSYS parametric design language to calculate the hot spot stress based on the extrapolation of the stress perpendicular to the weld. For the surface extrapolation, read-out points located at a distance equal to 0.4 and 1.4 times the chord thickness from the weld toe were used regardless of the location of the hot spot.

Contrary to the parametric finite element studies performed in the 1990s and early 2000s that used shell elements, more recent studies such as the ones performed by Shao et al. [33] and Ahmadi et al. [35], made use of three dimensional meshing elements. Although recommendations for using solid

elements and an explicitly modelled weld geometry to account for the local stiffness increase had already been formulated in the 1990s (e.g. [36]), the use of these elements for complete joint models in parametric studies was computationally not feasible back then. The increase of computing power in the last two decades has made parametric studies with 3D solid elements possible. The use hereof, combined with an explicitly modelled weld geometry produces significantly more accurate results than the use of shell elements [23]. Nonetheless, the SCF equations in the current design codes are still those derived from parametric studies using shell models. The same is true for SACS (Structural Analysis Computer System), which is one of the leading design software packages in the field of offshore engineering. The SCFs in SACS are a based on the Efthymiou equations. Other software packages that can be used for determination of the SCFs based on the hot spot stresses are FeSafe and nCode. Whilst both have implemented the surface stress extrapolation method, they are not optimized for the evaluation of tubular joints. An example is the DNV code which requires the hot spot stress to be determined as a maximum of three reference stresses. Furthermore, they require substantial user-input which can be detrimental in an industrial design context.

The framework (reported in section 4) was developed to be as robust as possible whilst requiring minimal (user) input. Its purpose is twofold. First, being fully automated means it lends itself to extensive parametric studies on the SCF distribution around the weld toe. Secondly, it is a powerful tool for designers to identify the fatigue critical locations in complex loaded joints. The algorithm takes into account the location of the weld toe with respect to

the chord and brace to determine the correct locations of reference points for surface stress extrapolation. It also considers the complete three-dimensional stress state at the weld toe, allowing for a more accurate calculation of the hot spot stress and thus of the SCFs. DNV-GL-RP203 [19] will be used as reference for the rest of this paper.

3. Finite element model

The first step is the development of a finite element model from which the output database is used as input for the developed framework. A static, linear elastic analysis needs to be performed using FEA to calculate the stresses for a certain load case. The most reliable results are obtained by including the weld geometry in the model, since the stiffening effect of the weld seam on chord wall bending is taken into account [37]. Including the weld in the geometry implies the use of three-dimensional meshing elements [19]. To obtain the most accurate results, quadratic 20 node brick elements with reduced integration and a size smaller than $0.5t$ should be used, where t is the local thickness. This recommendation is based on a comprehensive mesh sensitivity study of Kim et al. [16]. They used five different element types; an 8-node brick element with full and reduced integration, an 8-node brick element with an incompatible mode shape function and a 20-node brick element with a full and reduced integration. For all element types, four different mesh sizes ($0.1t/0.25t/0.5t/1.0t$) were used to model the area of the hot spot. The hot spot stress was obtained from linear extrapolation of surface stresses at $0.5t$ and $1.5t$ from the weld toe, for five different structural geometries. For the surface stress extrapolation method they concluded that

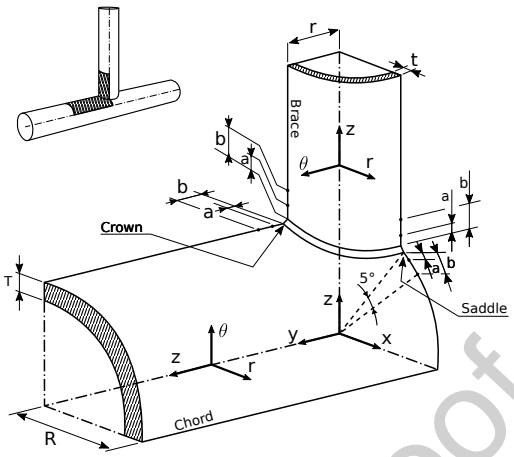

Figure 5: Read out points of stresses for derivation of the hot spot stresses in tubular joints as defined by DNV-GL-RP203 [19].

the quadratic element with reduced integration and a size smaller than $0.5t$ is recommended. An error less than 5% for both surface and edge hot spots was observed with respect to their convergence value. Their results are in line with the recommendations of DNV and IIW. Furthermore it has been shown that the use of solid brick elements produces more accurate results and a more detailed stress distribution near the intersection in comparison with shell elements [33, 35].

At both chord ends all degrees of freedom are fixed by applying the boundary conditions to a local reference point that is connected with a kinematic coupling to the free surface. The kinematic coupling constraints the nodes on the free surface to the rigid body motion of the reference point. The loads at the end of the brace are applied in a similar manner, but a distributed coupling is used to couple the reference point to the free surface at the brace end. The distributed coupling constrains the motion of the nodes on the

free surface to the translation and rotation of the reference point. This constraint is enforced in an average sense and in a way that enables control of the transmission of loads.

After meshing, a separate node set has to be defined for each brace and weld as well as for the chord of the tubular joint. These sets contain the nodes that lie on the surface of each feature. The nodes at the weld toe should be included in both the node set of the weld face as well as in the node set of the welded member. A local cylindrical coordinate system ($\mathbf{r}$, $\boldsymbol{\theta}$, $\mathbf{z}$) is assigned to each circular hollow section (CHS). By default, the stress components are associated with the global coordinate system ($\mathbf{x}$, $\mathbf{y}$, $\mathbf{z}$). By transforming the stress components in each CHS from the global coordinate system ($\mathbf{x}$, $\mathbf{y}$, $\mathbf{z}$) to its local cylindrical coordinate system ($\mathbf{r}$, $\boldsymbol{\theta}$, $\mathbf{z}$), only three in-plane stress components (σ_{zz}, $\sigma_{\theta\theta}$, and $\sigma_{z\theta}$) need to be extracted. Both the local cylindrical coordinate system and the global orthogonal coordinate system are illustrated in Fig. 5. For each node set that corresponds to a CHS, the nodal coordinates in the global coordinate system ($\mathbf{x}$, $\mathbf{y}$, $\mathbf{z}$) as well as the nodal stress components σ_{zz}, $\sigma_{\theta\theta}$, and $\sigma_{z\theta}$ associated with the local ($\mathbf{r}$, $\boldsymbol{\theta}$, $\mathbf{z}$) coordinate system of the CHS to which the node belongs are written to an ASCII file. For node sets corresponding to a weld, only the nodal coordinates need to be written to an ASCII file since the stresses in the weld are not used for the calculation of the hot spot stress calculation. The use of the ASCII format ensures that the developed framework can be used with different FEA packages. In other words, the developed framework works completely independent from the software that is used to perform the static analysis. The steps that are needed to generate the correct output

ASCII files are illustrated in flowchart Fig. 6. The generated ASCII files are used as the only input for the developed framework discussed in section 4.

4. Building blocks of the framework for automated hot spot stress calculation

4.1. Determination of the extrapolation directions

Since the input of the framework is merely a set of ASCII files containing the coordinates of the nodes in each user-defined node set, no actual geometrical parameters of the tubular joint are known. For each member of the tubular joint, the equation of its surface in the global coordinate system of the finite element model is determined. The sets of the circular hollow sections are three dimensional point clouds for which it is known that each point lies on the surface of a cylindrical surface. Therefore the node set surface can be described with a parametric equation. To determine the equation of each cylindrical surface, a least-squares minimization algorithm for fitting a cylinder to a set of points in a three-dimensional space can be used. Here the least-squares fitting algorithm as described in [38] is used. This algorithm is based on the assumption that the underlying data is modelled by a cylinder and that any possible errors have caused the data points not to be exactly on the cylinder. Since the surface nodes originate from a tubular joint mesh, this assumption will always be valid. The implemented fitting algorithm works for any arbitrary orientation of the global coordinate system, making it robust and thus ideal for this application. The use of such a robust fitting algorithm makes sure no requirements need to be specified with respect to the orientation of the global coordinate system in the FE modelling stage of

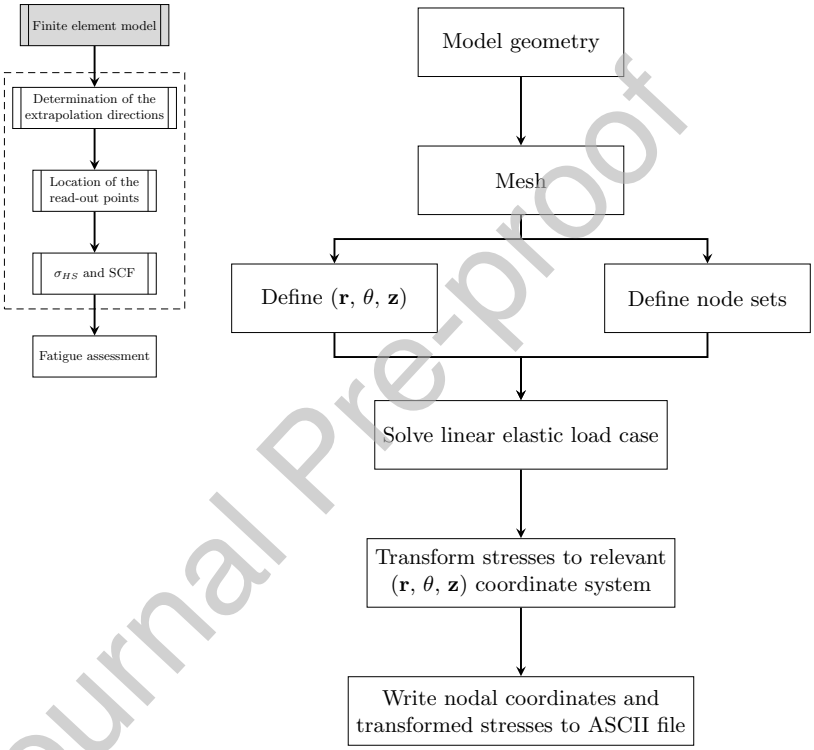

Figure 6: Flowchart of the steps needed to create the input for the developed framework based on finite element analysis.

the tubular joint since no assumptions about the orientation of the cylinder center axis are needed for the fitting algorithm to converge.

Before the coordinates of the read-out points for the stress extrapolation can be determined, a local coordinate system needs to be defined in each node on the considered weld toe line. This is illustrated in Fig. 7. The nodes that lie on the weld toe lines are determined by calculating the intersection between the node sets of the weld face and the node sets of the associated CHS. The local coordinate system in each node is defined by a set of three unit vectors ($\hat{\mathbf{n}}$, $\hat{\mathbf{t}}$, $\hat{\mathbf{b}}$). This set of unit vectors consists of the vector normal to the surface of the welded tubular joint member ($\hat{\mathbf{n}}$), the vector tangent to the weld toe ($\hat{\mathbf{t}}$) and the binormal vector ($\hat{\mathbf{b}}$), which is orthogonal to both $\hat{\mathbf{n}}$ and $\hat{\mathbf{t}}$ as defined in Eq. (1).

$$\hat{\mathbf{b}} = \hat{\mathbf{n}} \times \hat{\mathbf{t}} \tag{1}$$

First the normal vector $\mathbf{n}$ will be determined for all nodes on the weld toe. Hereto, the nodes of the considered weld toe are projected perpendicular on the center axis of the cylinder surface to which the considered weld toe belongs. Fig. 8a illustrates this projection for a weld toe on the chord surface. The equation of the center axis is known from the least-squares fitting of the cylinder. The normal unit vector $\hat{\mathbf{n}}$ for a node on the weld toe can be be computed based on the normalized vector defined by the node and its corresponding projection on the cylinder center axis. This can be expressed as follows. Assume that matrix $\boldsymbol{P}$ contains all nodal coordinates of the nodes on the considered weld toe; then $\boldsymbol{P}$ can be expressed as

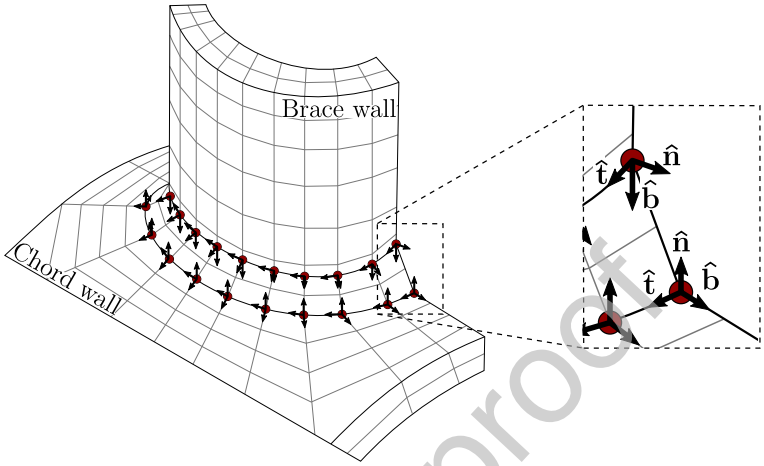

Figure 7: Local coordinate system at each weld toe node used to define the surface extrapolation direction. ($\hat{\mathbf{n}}$ = normal to tubular surface, $\hat{\mathbf{t}}$ = weld direction, $\hat{\mathbf{b}}$ = binormal).

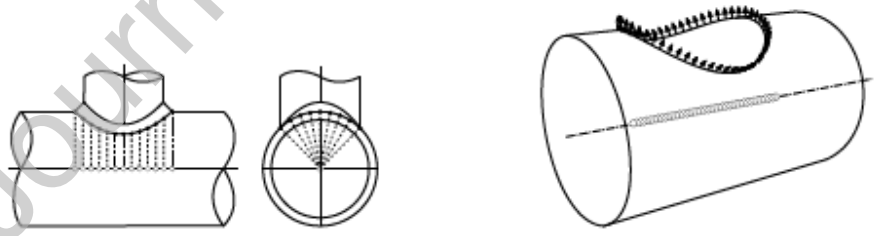

(a) Projection of the nodes on the chord weld toe line to the center axis of the chord member.

(b) Vectors normal to the chord weld toe line

Figure 8: Determination of the normal vectors to the chord surface on the weld toe line, illustrated for a T-joint configuration.

$$\boldsymbol{P} = \begin{bmatrix} P_1 & P_2 & \dots & P_n \end{bmatrix} \quad \text{with } P_i \in \mathbb{R}^3 \tag{2}$$

Consider the unit vector $\hat{\mathbf{c}}$ that coincides with the center axis of the considered CHS. The projection $\boldsymbol{Q}$ of the points in $\boldsymbol{P}$ can be calculated as

$$\begin{bmatrix} Q_1 & Q_2 & \dots & Q_n \end{bmatrix} = \begin{bmatrix} \hat{\mathbf{c}}\left(\hat{\mathbf{c}}^T P_1\right) & \hat{\mathbf{c}}\left(\hat{\mathbf{c}}^T P_2\right) & \dots & \hat{\mathbf{c}}\left(\hat{\mathbf{c}}^T P_n\right) \end{bmatrix} \quad \text{with } Q_i \in \mathbb{R}^3 \tag{3}$$

Eq. (3) can be more conveniently expressed as

$$\boldsymbol{Q} = \hat{\mathbf{c}}\,\hat{\mathbf{c}}^T \boldsymbol{P} \tag{4}$$

where $\boldsymbol{Q}$ contains the coordinates of the projected nodes that lie on the center axis of the considered CHS and $\hat{\mathbf{c}}\hat{\mathbf{c}}^T$ represents the projection matrix. Subtracting $\boldsymbol{Q}$ from $\boldsymbol{P}$, seen in Eq. (5), results in a matrix of which each element represents the vector normal to the cylindrical surface in the considered weld toe.

$$\boldsymbol{P} - \boldsymbol{Q} = \begin{bmatrix} \mathbf{n_1} & \mathbf{n_2} & \dots & \mathbf{n_n} \end{bmatrix} \quad \text{with } \mathbf{n_i} \in \mathbb{R}^3 \tag{5}$$

Normalizing each normal vector then results in the matrix $\boldsymbol{N}$, which contains the normal unit vectors for the considered weld toe line.

$$\boldsymbol{N} = \begin{bmatrix} \hat{\mathbf{n}}_1 & \hat{\mathbf{n}}_2 & \dots & \hat{\mathbf{n}}_n \end{bmatrix} \tag{6}$$

Fig. 8b illustrates the obtained normal vectors in $\boldsymbol{N}$ for a weld toe line on the chord surface. Next the tangent vector is determined. The unit tangent vector $\hat{\mathbf{t}}$ can be approximated by the relative position of the nodes at either

side of the considered node. Consider a node P_j that lies on the considered weld toe, the two closest neighbouring nodes P_i and P_k which also lie on the same weld toe are determined. P_i and P_k must lie on either side of P_j, thus the unit vector tangent to the weld toe line in P_j can be approximated by

$$\hat{\mathbf{t}} = \frac{P_i - P_k}{||P_i - P_k||} \tag{7}$$

When the normal vector and tangent vector in each node are determined, the binormal vector in each weld node can be computed using Eq. (1). The binormal vector serves as the basis for the determination of the coordinates of the read-out points (section 4.2) as it is parallel to the extrapolation direction. The flowchart in 9 summarizes the determination of the local coordinate systems in each weld toe node.

4.2. Determination of the read-out points

The direction of the binormal vector is not guaranteed to be the same as the required extrapolation direction. In order to determine the correct extrapolation direction for all weld toe nodes, a two step process is introduced. In the first step a distinction is made between nodes that lie on the surface of a brace and nodes that lie on the surface of the chord. For weld toe nodes on the chord, the correct extrapolation direction can be determined from the first step alone, the second step is therefore only applied to nodes that lie on a brace.

First a new unit vector, the surface vector $\hat{\mathbf{s}}$, is introduced. This is a normalized vector that initially coincides with the binormal vector. In the first step of the previously mentioned two step process the orientation of the surface

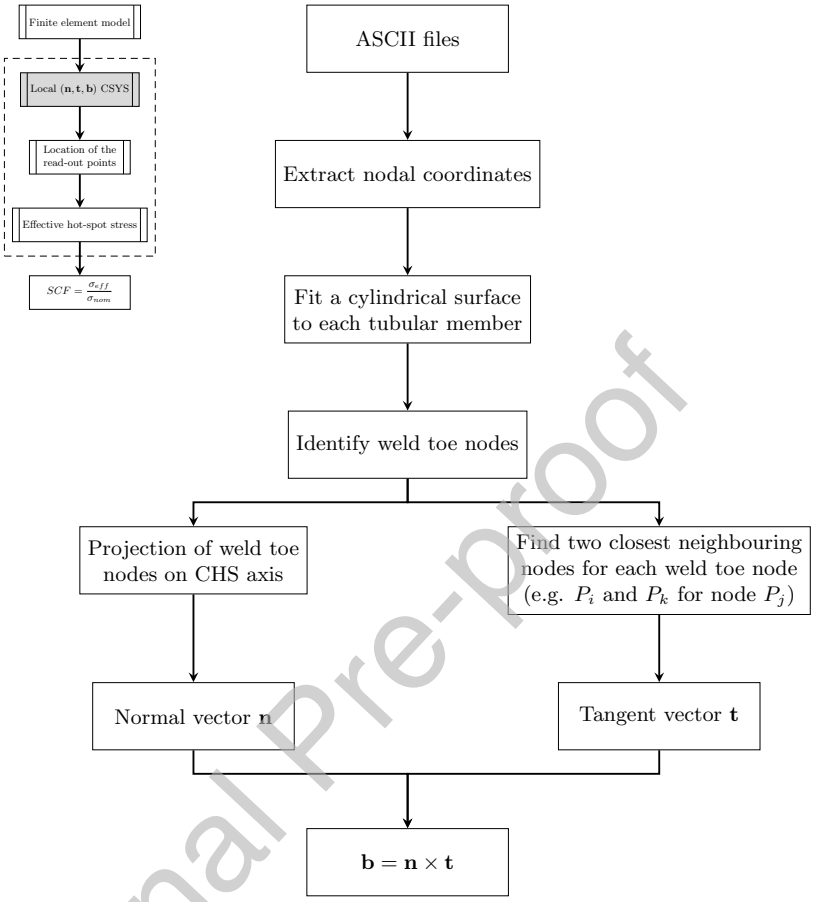

Figure 9: Determination of the local coordinate systems (CSYS) in each weld toe node. The local CSYS defines the surface extrapolation direction and is used for the future stress transformations.

vector in each node is compared to the orientation of a 'test vector' $\mathbf{a}$. The vector $\mathbf{a}$ is defined as the vector between the node and the center coordinate of all nodes on the weld toe, as is illustrated in Fig. 10. If the matrix $\boldsymbol{P} \in \mathbb{R}^{3\times n}$ contains the coordinates of all nodes that lie on the considered weld toe, then the center coordinate of the nodes on the weld toe is calculated

as

$$\mathbf{T} = \begin{bmatrix} \frac{\sum_{i=1}^{n} P_{1,i}}{n} \\ \frac{\sum_{i=1}^{n} P_{2,i}}{n} \\ \frac{\sum_{i=1}^{n} P_{3,i}}{n} \end{bmatrix} \tag{8}$$

where $\mathbf{T}$ is the center coordinate. The test vector $\mathbf{a}$ for each node on the considered weld toe line can then be calculated in a matrix form as

$$\begin{bmatrix} \mathbf{a_1} & \mathbf{a_2} & \dots & \mathbf{a_n} \end{bmatrix} = \mathbf{T} \begin{bmatrix} 1 & 1 & \dots & 1 \end{bmatrix} - \begin{bmatrix} P_1 & P_2 & \dots & P_n \end{bmatrix} \quad \text{with } \mathbf{a_i} \in \mathbb{R}^3 \tag{9}$$

where each element $\mathbf{a_i}$ represents a test vector. Next, for each weld node in $\boldsymbol{P}$ the dot product $\mathbf{a} \cdot \mathbf{s}$ is computed. If the dot product is positive, meaning the angle between the surface vector and the test vector is lower than 90°, the sense of the surface vector is reversed. Fig. 10a schematically shows the result for nodes that lie on a brace while Fig. 10b shows the orientation of the surface vectors before and after step 1 for nodes that lie on the chord.

Now consider $\boldsymbol{S}$, which contains all surface vectors of the considered weld toe node set as defined in Eq. (10).

$$\boldsymbol{S} = \begin{bmatrix} \mathbf{s_1} & \mathbf{s_2} & \dots & \mathbf{s_n} \end{bmatrix} \quad \text{with } \mathbf{s_i} \in \mathbb{R}^3 \tag{10}$$

The distinction between weld nodes that lie on a brace and weld nodes that lie on the chord can be made using the following equation:

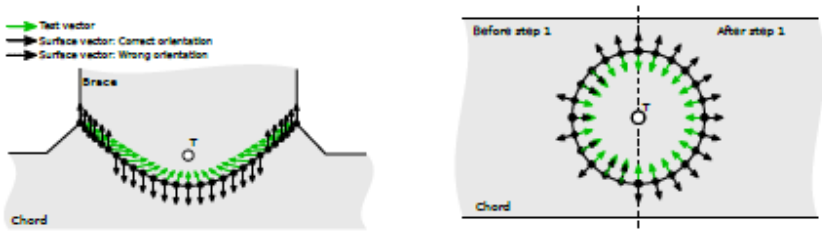

(a) Brace (sideview) (b) Chord (topview)

Figure 10: Illustration of the use of the test vector method to determine the correct surface extrapolation direction in each weld toe node.

$$f(\boldsymbol{S}) = \sum_{i=2}^{n} \begin{cases} 0 & , |\mathbf{s_1} \cdot \mathbf{s_i}| = 1 \\ |\mathbf{s_1} \cdot \mathbf{s_i}| & , otherwise \end{cases} \tag{11}$$

If Eq. (11) is equal to zero, all surface vectors of the corresponding nodes in the considered node set are parallel and thus the nodes lie on a brace (Fig. 10a). If on the other hand Eq. (11) does not equal zero, the situation corresponds to Fig. 10b, meaning the nodes lie on the chord. The surface vectors of the weld nodes that lie on the chord are correctly oriented, since for each node of the weld toe the corresponding surface vector coincides with the extrapolation direction for the determination of the read-out points. However, for weld nodes that lie on a brace this is not necessarily the case. To ensure that the surface vectors of the weld toe nodes that lie on a brace also coincide with the extrapolation direction, a second step is now introduced.

Consider matrix $\boldsymbol{A} \in \mathbb{R}^{3\times m}$ that contains only the nodes that lie on the surface of the considered brace and $\boldsymbol{P}$ that contains the nodes that lie on the considered weld toe. Using Eq. (12), a set of coordinates is determined that are used to check if the surface vector has the correct orientation or whether

it has to be reversed.

$$\boldsymbol{B} = \boldsymbol{P} + x\boldsymbol{S} \qquad with \quad \boldsymbol{B} \in \mathbb{R}^{3\times m} \tag{12}$$

The matrix $\boldsymbol{B}$ contains a set of points at an arbitrary distance x from the associated weld nodes in the direction of their respective surface vectors; x should be chosen such that it is larger than the average mesh size in the extrapolation zone. For each point in $\boldsymbol{B}$ the distance to the closest node in $\boldsymbol{A}$ is computed. If the computed distance is larger than the mesh size of the extrapolation zone, the point does not lie on the surface of the brace and thus the orientation of the surface vector has to be reversed. This procedure is illustrated in Fig. 11 where only the mesh of the brace is shown, since only the nodes that lie on the surface of the brace are considered in this step (i.e. the nodes in $\boldsymbol{A}$).

For weld nodes that lie on a brace, the coordinates of the read-out points at an arbitrary distance x from the weld node can now be determined using Eq. (13).

$$\boldsymbol{R} = \boldsymbol{A} + x\boldsymbol{S} \qquad with \quad \boldsymbol{R} \in \mathbb{R}^{3\times m} \tag{13}$$

DNV-GL-RP203 recommends two read-out points for the extrapolation of the stress components along the brace surface normal to the weld toe (i.e. along the surface vector) as can be seen in Fig. 5. The extrapolation distances recommended by DNV-GL-RP203 are reported in Table 1.

The determination of the coordinates of the read-out points that lie on the chord is less straight-forward. The DNV recommended practice distinguishes

Table 1: Read-out point locations recommended by DNV-GL-RP203 [19]

Brace	Chord (crown)	Chord (saddle)
$a = 0.2\sqrt{rt}$	$a = 0.2\sqrt{rt}$	$a = 0.2\sqrt{rt}$
$b = 0.65\sqrt{rt}$	$b = 0.4\sqrt[4]{rtRT}$	$b = \frac{\pi R}{36}$

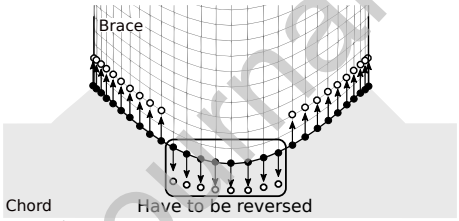

Figure 11: Determination of the surface vector direction for weld nodes on a brace. Only the nodes on the surface of the brace are considered.

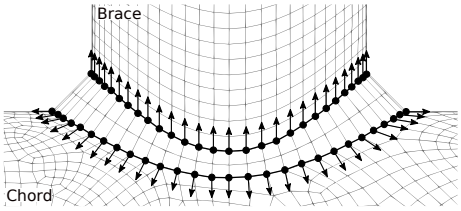

Figure 12: Surface vectors at the brace and chord weld toe nodes after application of both surface vector orientation checks.

two characteristic locations for the determination of the hot spot stress, the crown and saddle positions (see Fig. 5). For each of these locations the second extrapolation point lies at a different distance from the weld toe. For the weld node at the crown, the read-out points follow immediately from Eq. (13) since the surface vector is both perpendicular to the weld and coincident with the cylinder surface. For all other nodes that lie on the same weld toe, the surface vector is tangential to the surface of the chord, thus using Eq. (13) for any node other than the node at the crown position results in a read-out point that is positioned at an offset from the surface of the chord, as is illustrated in Fig. 13.

As mentioned in the introduction, the hot spot stresses are generally only computed for a few critical locations on the circumference of the weld toe. Since DNVGL-RP-203 does not provide recommendations with respect to the location of the read out points for nodes that do not lie on these critical locations, the following is proposed. For each considered weld node the angle α between its surface vector and the center axis of the chord is computed. Based on the computed angle the extrapolation distance is then determined as illustrated in Fig. 13. For the nodes in the grey zone ('saddle region'), the extrapolation distance for the saddle is used, in the other zone ('crown region') the distance formula of the crown is used.

Fig. 14 illustrates how the correct read-out points are determined for a weld node in case Eq. (13) results in read-out points that are offset from the surface. First the points A and B are computed, which lie along the surface vector $\mathbf{s}$ using Eq. (13). Here x respectively equals to $|OA|$ and $|OB|$. A and

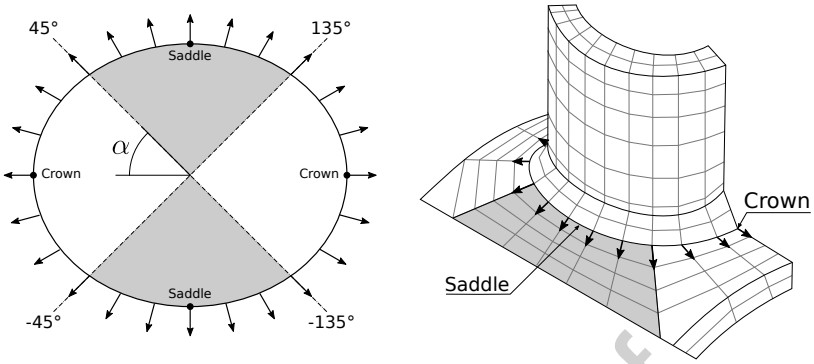

Figure 13: Determination of the extrapolation regions based on the angle between the surface vector and the center axis of the chord.

B are then projected perpendicularly on the chord surface. In order for the positions of a and b to correspond to the values recommended by DNV-GL-RP203, $|OA|$ and $|OB|$ have to be calculated using equations Eq. (14) and Eq. (15) for nodes that lie in the region of the saddle. For nodes that lie in the region of the crown, the equations as proposed by DNV-GL-RP203, tabulated in Table 1 can be used. 15 summarizes how the locations of the read-out points are determined as discussed in this subsection.

$$|OA| = R\,tan\left(\frac{0.2\sqrt{rt}}{t}\right) \tag{14}$$

$$|OB| = R\,tan\left(5°\frac{\pi}{180}\right) \tag{15}$$

4.3. Calculation of the hot spot stresses

Once the coordinates of the read-out points have been determined, the stresses at the hot spot can be calculated. First the stress components $\sigma_{\theta\theta}$, σ_{zz}, and $\sigma_{z\theta}$ need to be extracted at the read-out points associated with the hot spot. For read-out points that coincide with a node from the mesh of the considered

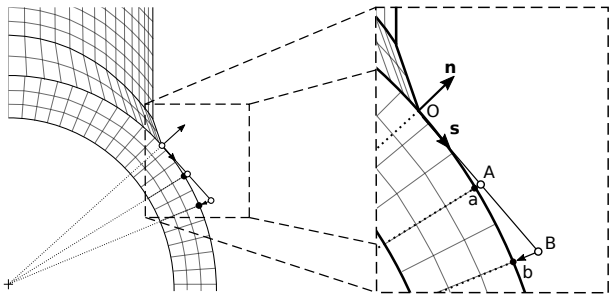

Figure 14: Determination of the extrapolation distance for nodes on the weld toe of the chord that do not lie at the crown, illustrated for a node at the saddle point.

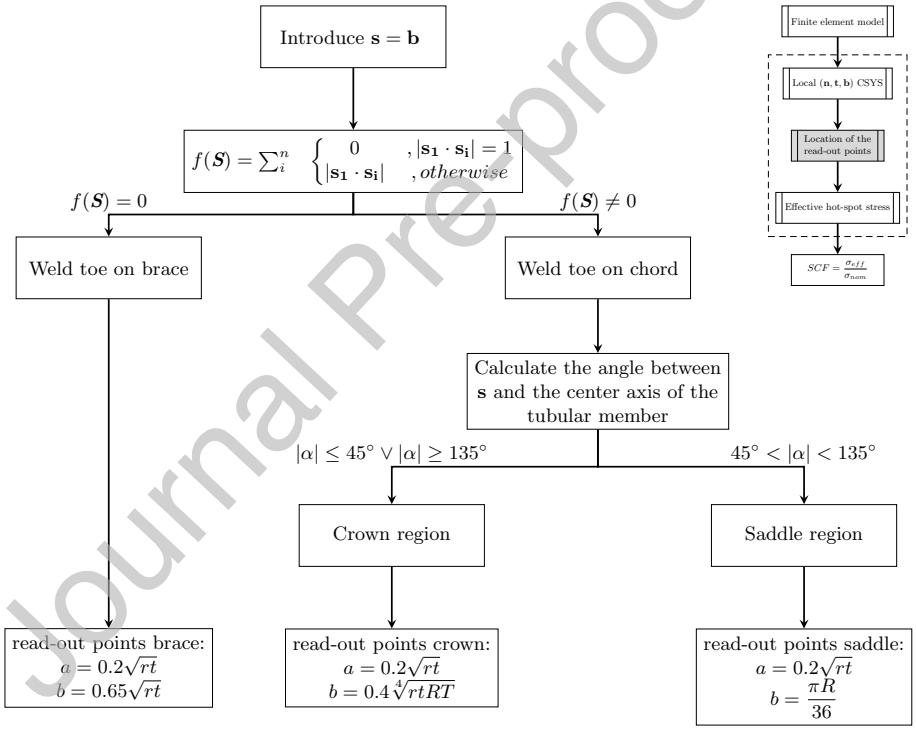

Figure 15: Determination of the read-out points based on the extrapolation vector and the geometric parameters of the tubular joint.

CHS, the stress components in that node are extracted. If the read-out point does not coincide with an existing node, the stress components of the two closest neighbouring nodes along the extrapolation direction are extracted and averaged. If the mesh is irregular in the extrapolation region, the choice can be made to select the three closest neighbouring nodes to achieve a more accurate averaged stress. Ideally the mesh of the finite element model should be designed such that the read-out points coincide with the nodes of the mesh. The individual stress components are now extrapolated parallel to the surface vector, towards the hot spot. This is illustrated in Fig. 16. The framework can be used to evaluate different approaches for hot spot stress calculation since the stresses that are extrapolated to the hot spot (principal stresses, perpendicular stress, stress tensor) and the corresponding effective hot spot stress calculation can be easily adapted.

Following the recommended practice of DNV, an effective hot spot stress range $\Delta\sigma_{HS}$ (in [19] denoted to as $\Delta\sigma_{eff}$) has to be calculated for fatigue assessments based on the following equations.

$$\Delta\sigma_{HS} = max \begin{cases} \sqrt{\Delta\sigma_{\perp}^2 + 0.81\Delta\tau_{/\!/}^2} \\ |\Delta\sigma_1| \\ |\Delta\sigma_2| \end{cases} \tag{16}$$

Here $\Delta\sigma_1$ and $\Delta\sigma_2$ are the in-plane principal stress ranges at the hot spot, $\Delta\sigma_{\perp}$ is the range of the normal stress perpendicular to the weld toe and $\Delta\tau_{\parallel}$ is the shear stress range. The first term of Eq. (16) is there to account for the situation where fatigue cracking occurs along the weld toe. When fatigue cracking occurs more perpendicular to the weld, one of the in-plane principal

stresses will be maximal [19]. The different stress components for an element in front of the weld toe are are illustrated in Fig. 17. The principal stress ranges $\Delta\sigma_1$ and $\Delta\sigma_2$ can be calculated as

$$\Delta\sigma_1 = \frac{\Delta\sigma_\perp + \Delta\sigma_{/\!/}}{2} + \frac{1}{2}\sqrt{\left(\Delta\sigma_\perp - \Delta\sigma_{/\!/}\right)^2 + 4\Delta\tau_{/\!/}^2} \tag{17}$$

$$\Delta\sigma_2 = \frac{\Delta\sigma_\perp + \Delta\sigma_{/\!/}}{2} - \frac{1}{2}\sqrt{\left(\Delta\sigma_\perp - \Delta\sigma_{/\!/}\right)^2 + 4\Delta\tau_{/\!/}^2} \tag{18}$$

where $\Delta\sigma_\parallel$ is the normal stress range parallel to the weld toe. Fig. 16 shows that the stress components at the hot spot that are oriented along the local ($\mathbf{r}$, $\boldsymbol{\theta}$, $\mathbf{z}$) coordinate system, do not coincide with the directions perpendicular and parallel to the weld for nodes that are not located at the saddle or crown locations. Although the principal stresses can be calculated using the known ($\mathbf{r}$, $\boldsymbol{\theta}$, $\mathbf{z}$) stress components, the first term in Eq. (16) cannot. Since $\Delta\tau_\parallel$ and $\Delta\sigma_\perp$ coincide with the local ($\mathbf{n}$, $\mathbf{t}$, $\mathbf{s}$) coordinate system in each weld node, they can be calculated by transforming the ($\mathbf{r}$, $\boldsymbol{\theta}$, $\mathbf{z}$) stress components to the ($\mathbf{n}$, $\mathbf{t}$, $\mathbf{s}$) coordinate system. The stresses $\tau_\parallel$ and $\sigma_\perp$ are calculated as

$$\sigma_{/\!/} = \frac{\sigma_{\theta\theta} + \sigma_{zz}}{2} + \frac{\sigma_{\theta\theta} - \sigma_{zz}}{2} cos(2\,\phi) + \tau_{z\theta} sin(2\,\phi) \tag{19}$$

$$\sigma_\perp = \frac{\sigma_{\theta\theta} + \sigma_{zz}}{2} - \frac{\sigma_{\theta\theta} - \sigma_{zz}}{2} cos(2\,\phi) - \tau_{z\theta} sin(2\,\phi) \tag{20}$$

$$\tau_{/\!/} = -\frac{\sigma_{\theta\theta} - \sigma_{zz}}{2} sin(2\,\phi) + \tau_{z\theta} cos(2\,\phi) \tag{21}$$

here ϕ is the angle between the surface vector $\mathbf{s}$ and the $\boldsymbol{\theta}$ axis of the ($\mathbf{r}$, $\boldsymbol{\theta}$, $\mathbf{z}$) coordinate system (see Fig. 17). Once the hot spot stress in each weld node is known, the SCF distribution can be obtained by dividing σ_{HS} in each node

by σ_{nom}. The steps presented in this section are illustrated in the flowchart Fig. 18.

5. Case studies

5.1. Validation for a uni-planar T-type joint

To validate the developed framework, a finite element model of a uni-planar tubular T-joint was constructed. Three principal load cases were simulated; namely axial loading, in-plane bending and out-of-plane bending. The experimental study of Yeoh et al. [29] and the subsequent numerical study of Soh [18] were used as a reference for the geometry as this allows for a comparison of results. Fig. 19 shows the configuration and dimensions of the model with the corresponding dimensionless geometrical parameters. The finite element simulation is purely linear elastic, the material parameters used for the steel grade are E = 210GPa and $\nu = 0.3$.

All models were developed in the FEA software Abaqus/CAE 2019. Based on the results of the mesh sensitivity study of Kim et al. [16] discussed in section 3 and the recommendations of DNV, quadratic brick elements with a reduced integration scheme (C3D20R) were selected. The mesh size in the surface stress extrapolation zone was chosen as $0.25t$ in order to achieve a good mesh quality without distorted elements. To reduce the computation time, the mesh density was decreased further away from the region of interest, four elements where used throughout the thickness of the complete model. The mesh is illustrated in Fig. 20. For the validation, the weld geometry was not explicitly modelled as this was also the case in the numerical model of Soh [18] and information on the weld geometry of the tubular joint that

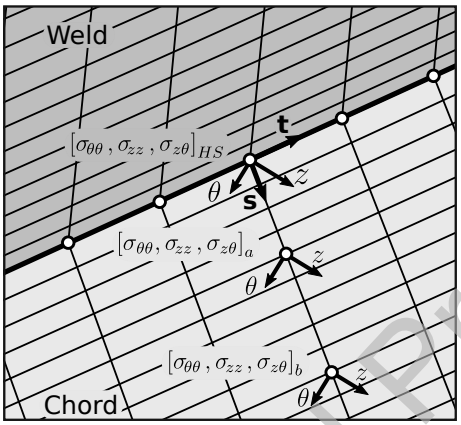

Figure 16: Extrapolation of ($\mathbf{r}$, $\boldsymbol{\theta}$, $\mathbf{z}$) stress components to the hot spot using the surface vector s, illustrated for an arbitrary location between the saddle and crown locations on the circumference of the weld toe.

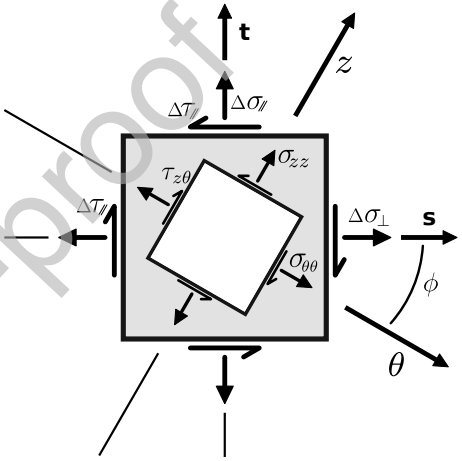

Figure 17: The relevant stress components for an element in front of the weld toe. The angle ϕ is used to transform the stress components in the cylindrical CSYS to the local (n, t, s) CSYS.

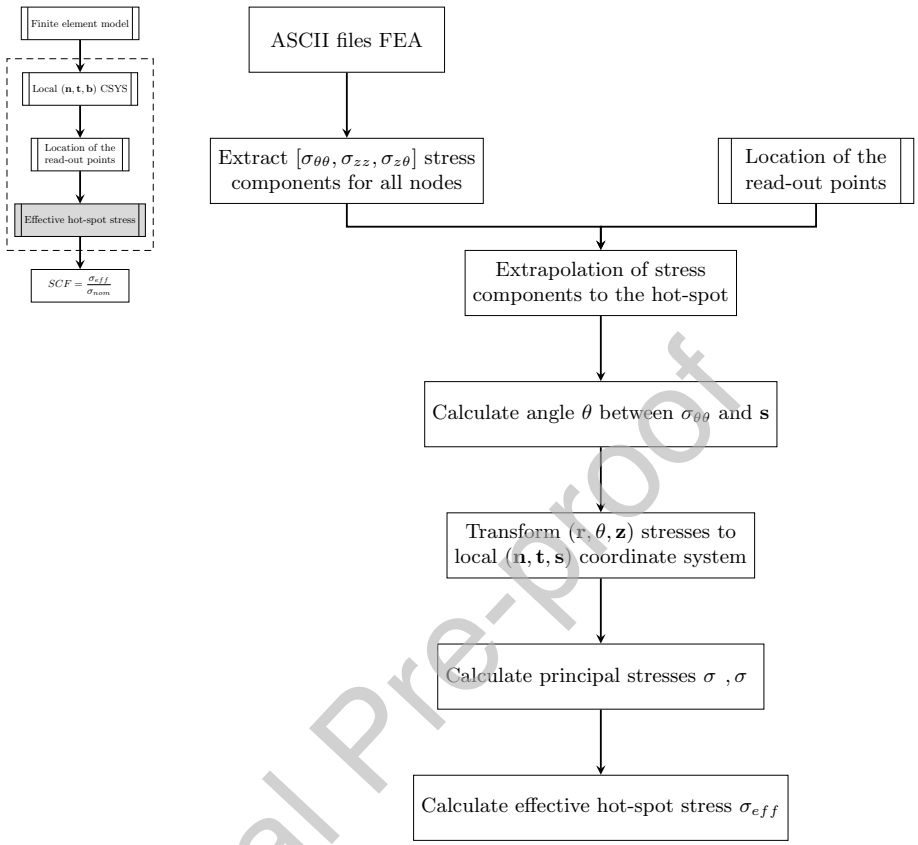

Figure 18: Calculation of the effective hot spot stress from the extrapolated stress components at the weld toe nodes based on the DNV recommended practice.

was used in the experimental study has not been reported in either of the references [29, 18]. Loads and boundary conditions were applied as described in section 3. For the axial load case a reference load of 1 kN was used, for the IPB and OPB load cases a reference load of 1 kNm was used.

The SCF is calculated as the ratio of the local surface stress at the brace-to-chord intersection (i.e. the hot spot stress) to the nominal stress in the brace. In case of axial loading the nominal stress $\sigma_{n,ax}$ is equal to the applied

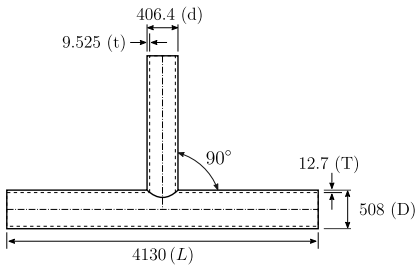

Figure 19: Model dimensions (in mm)

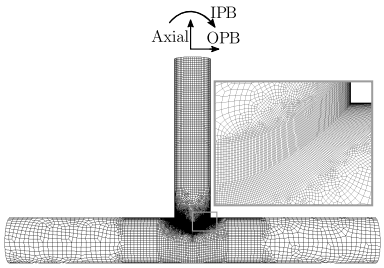

Figure 20: Global view of the mesh

force divided by the cross sectional area of the brace:

$$\sigma_{n,ax} = \frac{4F}{\pi \left[d^2 - (d-2t)^2\right]} \tag{22}$$

for in-plane or out-of-plane bending the nominal stress $\sigma_{n,b}$ is calculated as:

$$\sigma_{n,b} = \frac{32dM}{\pi \left[d^4 - (d-2t)^4\right]} \tag{23}$$

Fig. 22 shows comparisons between the results obtained using the framework described in section 4, the experimental results reported by Soh [29] and the parametric equations of Hellier [31] that describe the SCF distribution along the circumference of the intersection. For each principal loading case the SCF distributions at the weld toe on the brace and at the weld toe on the chord are shown. For this comparison the weld geometry was not explicitly taken into account as shown in Fig. 20. The SCF distributions were calculated based on extrapolation from both the chord and brace surface with respect to the intersection between of the brace the chord.

The results obtained using the developed framework show a better agreement with the experimental results of Soh [29] compared to the the equations of

Hellier [31]. In Fig. 22b significant discrepancies can be seen between the experimental results (especially at the chord crown) and both the present work and the equations of Hellier. The presented framework however is able to capture the high stress concentrations that occur at the saddle on the chord during axial load (Fig. 22b), which would be the most damaging for the load case, whilst the equations of Hellier do not. Discrepancies between the experimental results of Soh [29] and the present results are to be expected. Soh does not report the exact locations of the strain gauges with respect to the weld toe in his original work. There is also no report made of the weld geometry or weld quality that was used to connect the brace and chord in the experimental set-up. Soh also reports several inaccurate measurements, for example on Fig. 22a at 45 deg and 180 deg. Disregarding the outliers of the experimental data and taking uncertainties due to a lack of knowledge about the experimental conditions into account, the results presented in Fig. 22 show a good agreement with the experimental results. Fig. 22a, 22c, 22e and 22f show that the current algorithm is able to capture the shape of the SCF distributions originating from the experimental measurements results very well.

5.2. Influence of including the weld geometry on the SCF calculations

The model presented in the previous section was also extended with a weld geometry to gain insight into the importance of including the actual weld geometry in the finite element model. The weld dimensions used were determined based on the recommendations of standard AWS D1.1/D1.1M:2015 [21] for complete joint penetration (CJP) weld configuration. The AWS standard specifies how the dimensions of the weld vary around the brace-to-chord

intersection as a function of the local dihedral angle Ψ. The angle Ψ is defined as the angle between the chord and brace surface measured at the location of interest around intersection between chord and brace.

The calculated SCF distribution along the weld toe along the weld toe lines are shown in Fig. 21 for the three basic loading cases. Overall the influence of the weld geometry on the SCF distribution seems rather limited for the chosen joint. The most significant influence can be observed in the case of IPB (Fig. 21c and 21d) where the highest SCF occurs at the crown. The addition of the weld geometry to the finite element model results in a 10.2% decrease of the maximal SCF at the weld toe on the chord for IPB. Although the overall influence observed in this case study is limited, other researchers report larger discrepancies [23, 39]. For example, Lozano-Minguez et al. [23] studied the effects of the weld geometry on the SCFs at the crown and saddle points for a T-joint and reported a difference of 61.1% for axial loading, 64.3% for IPB and 56.5% for OPB. The reason that smaller SCF differences are found in this study can be explained by the large d/D ratio of the model used in this study (d/D =0.8) compared to that of the model used in the study of Lozana-Minguez et al. (d/D =0.5). The large value of the d/D ratio means that the geometrical difference between a tubular joint model without weld and with weld is limited; in other words, only a limited amount of weld material is added. The joint geometry studied by Lozano-Minguez et al. requires a larger weld volume, this results in a larger increase of the local wall thickness and thus of the local stiffness.

6. Conclusion

A numerical framework that allows for automated calculation of the hot spot stress and SCF distribution along the brace-to-chord intersection weld of a tubular joint was presented. It was developed to be fully independent of the finite element package that is used to perform the linear elastic stress analysis from which the results are used as an input. The developed framework consists of three main building blocks. First a local coordinate system (determined by vectors normal to the brace or chord, tangential to the weld and binormal) has to be defined in each weld toe node. The coordinate system is used in the second step to find the location of the read-out points and the extrapolation direction of the associated weld toe node. When the read-out points associated with each weld toe node are known, the individual stress components at the read-out points are extrapolated towards the hot spot. The hot spot stress is then calculated in each weld toe node based on the complete stress tensor, thus taking into account the in-plane normal and shear stresses. The SCF distribution is finally calculated as the ratio of the hot spot stresses σ_{HS} to the nominal stress σ_{nom} in the brace.

The hot spot stress approach is often applied by extrapolation of the maximum principal stress values at the read-out points. But for complex loading conditions the orientations of the principal stress vectors at both read-out points are not guaranteed to coincide. Therefore in the presented framework the complete stress tensor is extrapolated to the hot spot. By calculating the hot spot stress from the individually extrapolated in-plane stress components a more accurate and physically sound representation is obtained. This

makes the presented method a powerful tool for assessment of tubular joints subjected to multi-axial loads.

In order to validate the developed framework, SCF distributions along the weld toe lines of a T-joint were calculated for three basic load cases (axial loading, in-plane bending, out-of-plane bending). Results from the proposed framework were compared to experimental data and equations reported in literature. The results presented in this paper show that the developed framework is capable of accurately capturing the SCF distribution. Finally, a preliminary case study showed that including the weld geometry in the geometrical model can have a significant effect on the SCF distribution and therefore also on the fatigue life. The framework discussed in this paper can be integrated in a more comprehensive fatigue design framework [40], allowing for detailed studies of the effects of weld geometries and complex loading cases on fatigue life of offshore tubular joints.

7. Acknowledgements

The authors acknowledge the financial support of Vlaio through the SafeLife project (project number 179P04718W).

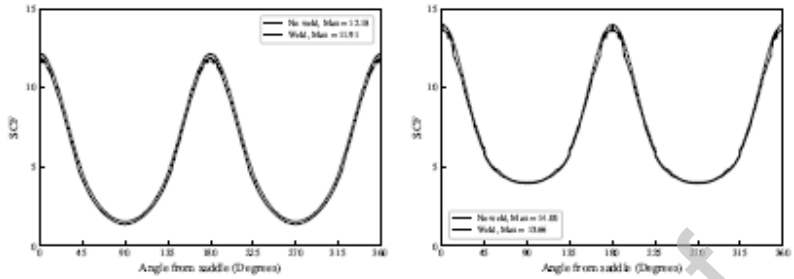

(a) Extrapolation in brace surface parallel to brace (b) Extrapolation in chord surface parallel to weld axis

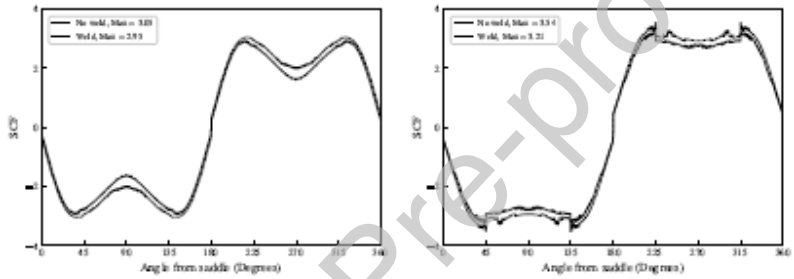

(c) Extrapolation in brace surface parallel to brace (d) Extrapolation in chord surface parallel to weld axis

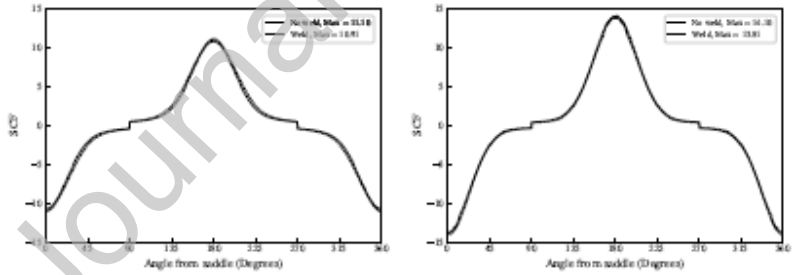

(e) Extrapolation in brace surface parallel to brace (f) Extrapolation in chord surface parallel to weld axis

Figure 21: Stress concentration factor (SCF) distribution at the chord/brace intersection for a T-joint FEA model with and without weld geometry subjected to an axial load (a, b), in-plane bending (IPB) (c, d) and out-of-plane bending (OPB) (e, f)

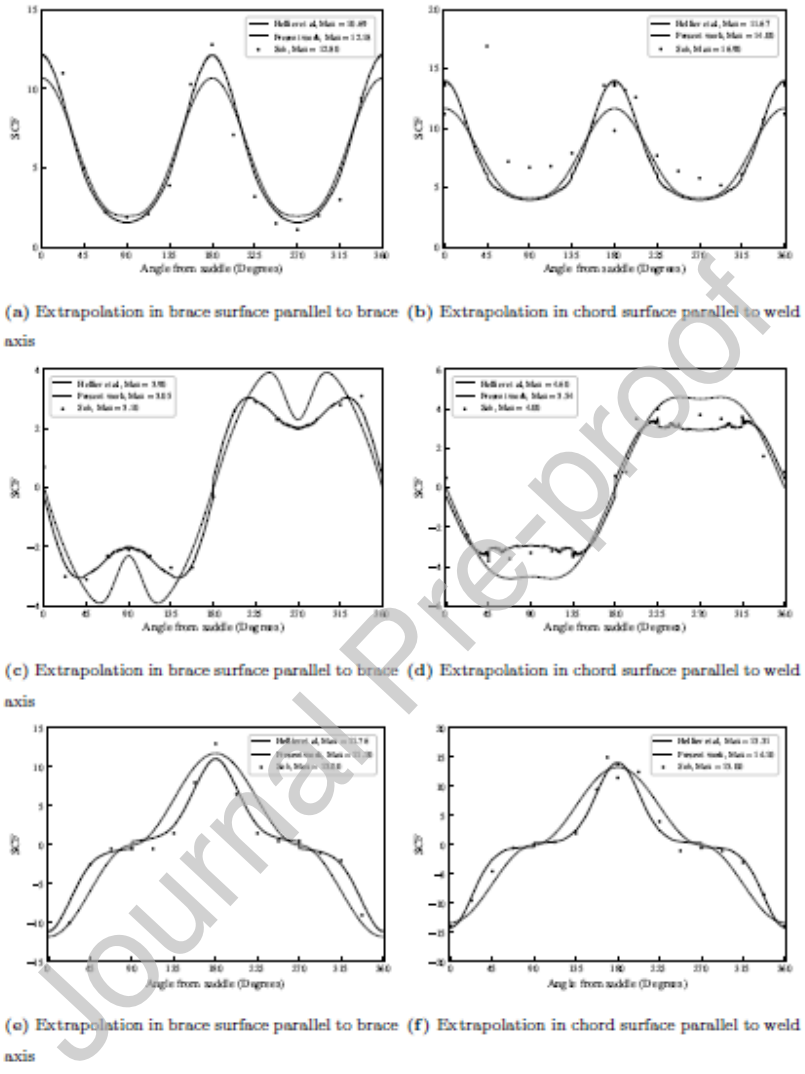

(a) Extrapolation in brace surface parallel to brace (b) Extrapolation in chord surface parallel to weld axis

(c) Extrapolation in brace surface parallel to brace (d) Extrapolation in chord surface parallel to weld axis

(e) Extrapolation in brace surface parallel to brace (f) Extrapolation in chord surface parallel to weld axis

Figure 22: Stress concentration factor (SCF) distributions at the chord/brace intersection determined using the presented framework are compared to the HCD equation and the experimental results reported by Soh et al. for a T-joint subjected to an axial load (a, b), in-plane bending (IPB) (c, d) and out-of-plane bending (OPB) (e, f)

References

[1] C. Devriendt, F. Magalhães, W. Weijtjens, G. De Sitter, Á. Cunha, P. Guillaume, Structural health monitoring of offshore wind turbines using automated operational modal analysis, Structural Health Monitoring 13 (6) (2014) 644–659. doi:10.1177/1475921714556568.

[2] A review of multiaxial fatigue criteria for random variable amplitude loads, Fatigue and Fracture of Engineering Materials and Structures 40 (7) (2017) 1007–1036. doi:10.1111/ffe.12619.

[3] European Union, Eurocode 3: Design of steel structures - Part 1-9: Fatigue, Tech. rep. (2011).

[4] E. Niemi, W. Fricke, S. J. Maddox, Structural Hot-Spot Stress Approach to Fatigue Analysis of Welded Components, 2nd Edition, Springer, 2018. doi:10.1007/978-981-10-5568-3.

[5] I. Poutiainen, P. Tanskanen, G. Marquis, Finite element methods for structural hot spot stress determination - A comparison of procedures, International Journal of Fatigue 26 (11) (2004) 1147–1157. doi:10.1016/j.ijfatigue.2004.04.003.

[6] Evaluation of fatigue damage model predictions for fixed offshore wind turbine support structures, International Journal of Fatigue 87 (2016) 71–80. doi:10.1016/j.ijfatigue.2016.01.007.

[7] H. Ahmadi, M. A. Lotfollahi-Yaghin, M. H. Aminfar, Stress concentration factors at saddle and crown positions on the central brace of two-

planar welded CHS DKT-connections, Journal of Marine Science and Application 11 (1) (2012) 83–97. doi:10.1007/s11804-012-1109-2.

[8] S. Manson, Fatigue : A Complex Subject-Some Simple Approximations some approximations useful in design are outlined and their application illustrated, Experimental Mechanics 5 (4) (1965) 193–226. doi:10.1007/BF02321056.

[9] P. Dong, A structural stress definition and numerical implementation for fatigue analysis of welded joints, International Journal of Fatigue 23 (10) (2001) 865–876. doi:10.1016/S0142-1123(01)00055-X.

[10] S. J. Maddox, Hot-spot stress design curves for fatigue assessment of welded structures, International Journal of Offshore and Polar Engineering 12 (2) (2002) 134–141.

[11] O. Doerk, W. Fricke, C. Weissenborn, Comparison of different calculation methods for structural stresses at welded joints, International Journal of Fatigue 25 (5) (2003) 359–369. doi:10.1016/S0142-1123(02)00167-6.

[12] J.-M. Lee, J.-K. Seo, et al., Comparison of hot spot stress evaluation methods for welded structures, International Journal of Naval Architecture and Ocean Engineering 2 (4) (2010) 200–210. doi:10.2478/IJNAOE-2013-0037.

[13] P. Dong, A robust structural stress method for fatigue analysis of offshore/marine structures, Journal of Offshore Mechanics and Arctic Engineering 127 (1) (2005) 68–74. doi:10.1115/1.1854698.

[14] P. Dong, J. K. Hong, Fatigue of Tubular Joints: Hot Spot Stress Method Revisited, Journal of Offshore Mechanics and Arctic Engineering 134 (3) (2012) 031602. doi:10.1115/1.4005188.

[15] D. S. Saini, D. Karmakar, S. Ray-Chaudhuri, A review of stress concentration factors in tubular and non-tubular joints for design of offshore installations, Journal of Ocean Engineering and Science 1 (3) (2016) 186–202. doi:10.1016/j.joes.2016.06.006.

[16] Y. Kim, J. S. Oh, S. H. Jeon, Novel hot spot stress calculations for welded joints using 3D solid finite elements, Marine Structures 44 (2015) 1–18. doi:10.1016/j.marstruc.2015.07.004.

[17] A. M. van Wingerde, J. A. Packer, J. Wardenier, Criteria for the fatigue assessment of hollow structural section connections, Journal of Constructional Steel Research 35 (1) (1995) 71–115. doi:10.1016/0143-974X(94)00030-I.

[18] A. K. Soh, An improved procedure for the determination of hot spot stresses in tubular joints, Fatigue and Fracture of Engineering Materials and Structures 20 (12) (1997) 1709–1718. doi:10.1111/j.1460-2695.1997.tb01523.x.

[19] DNV GL, DNVGL-RP-203: Fatigue design of offshore structures, Tech. Rep. DNVGL-RP-C203, DNV GL, Oslo (2016).

[20] X. L. Zhao, S. Herion, P. J.A., R. S. Puthli, G. Sedlacek, J. Wardenier, K. Weynand, A. M. van Wingerde, N. F. Yeomans, Design guide:

for circular and rectangular hollow section welded joints under fatigue loading, Tech. rep., Germany (2001).

[21] American Welding Society (AWS), AWS D1.1 Structural welding - Steel , Tech. rep.

[22] American petroleum Institute, Recommended practice for planning, designing and constructing fixed offshore platforms, Tech. Rep. 22nd edition (2014).

[23] E. Lozano-Minguez, F. P. Brennan, A. J. Kolios, Reanalysis of offshore T-joint fatigue life predictions based on a complete weld profile model, Renewable Energy 71 (2014) 486–494. doi:10.1016/j.renene.2014.05.064.

[24] A. C. Wordsworth, G. P. Smedley, Stress concentrations at unstiffened tubular joints, in: Proceedings of the European Offshore Steels Research Seminar, UK Dept of Energy by the Welding Institute, Cambridge, UK, 1978.

[25] Lloyd's Register of Shipping, Stress concentration factor for simple tubular joints - Assessment of existing and development of new parametric formulae, Tech. rep., London, UK (1997).

[26] J. G. Kuang, A. B. Potvin, R. D. Leick, Stress concentration in tubular joints, Proceedings of the Annual Offshore Technology Conference 1975-May (1975) 593–603. doi:10.2118/5472-PA.

[27] M. Efthymiou, S. Durkin, Stress concentrations in T/Y and gap/overlap

K-joints, in: Proceedings of the 4th International Conference on Behaviour of Offshore Structures, British Maritime Technology, Delft, The Netherlands, 1985, p. 429.

[28] B. M. R. Morgan, M. M. K. Lee, Stress concentration factors in tubular K-joints under in-plane moment loading, Journal of structural engineering 124 (4) (1998) 382–390. doi:10.1061/(ASCE)0733-9445(1998)124:4(382).

[29] S. K. Yeoh, A. K. Soh, C. K. Soh, Behaviour of tubular T-joints subjected to combined loadings, Journal of Constructional Steel Research 32 (3) (1995) 259–280. doi:10.1016/0143-974X(95)93898-E.

[30] H. L. Pang, C. W. Lee, Three-dimensional finite element analysis of a tubular T-joint under combined axial and bending loading, International Journal of Fatigue 17 (5) (1995) 313–320. doi:10.1016/0142-1123(95)00019-P.

[31] A. K. Hellier, M. P. Connolly, W. D. Dover, Stress concentration factors for tubular Y- and T-joints, International Journal of Fatigue 12 (1) (1990) 13–23. doi:10.1016/0142-1123(90)90338-F.

[32] E. Chang, W. D. Dover, Prediction of stress distributions along the intersection of tubular Y and T-joints, International Journal of Fatigue 21 (4) (1999) 361–381. doi:10.1016/S0142-1123(98)00083-8.

[33] Y. B. Shao, Z. F. Du, S. T. Lie, Prediction of hot spot stress distribution for tubular K-joints under basic loadings, Journal of Constructional Steel

Research 65 (10-11) (2009) 2011–2026. doi:10.1016/j.jcsr.2009.05.004.

[34] M. A. Lotfollahi-Yaghin, H. Ahmadi, Effect of geometrical parameters on SCF distribution along the weld toe of tubular KT-joints under balanced axial loads, International Journal of Fatigue 32 (4) (2010) 703–719. doi:10.1016/j.ijfatigue.2009.10.008.

[35] H. Ahmadi, M. A. Lotfollahi-Yaghin, Stress concentration due to in-plane bending (IPB) loads in ring-stiffened tubular KT-joints of offshore structures: Parametric study and design formulation, Applied Ocean Research 51 (2015) 54–66. doi:10.1016/j.apor.2015.02.009.

[36] S. A. Karamanos, A. Romeijn, J. Wardenier, Stress concentrations in multi-planar welded CHS XX-connections, Journal of Constructional Steel Research 50 (3) (1999) 259–282. doi:10.1016/S0143-974X(98)00244-2.

[37] C. M. Sonsino, Comparison of different local design concepts for the structural durability assessment of welded offshore K-nodes, International Journal of Fatigue 34 (1) (2012) 27–34. doi:10.1016/j.ijfatigue.2010.09.005.

[38] D. Eberly, Least Squares Fitting of Data by Linear or Quadratic Structures, Chapel Hill, NC: Magic Software (2018) 38–51.

[39] J. Maheswaran, S. C. Siriwardane, Fatigue life estimation of tubular joints - A comparative study, Fatigue and Fracture of Engineering Materials and Structures 39 (1) (2016) 30–46. doi:10.1111/ffe.12314.

[40] K. Hectors, H. De Backer, M. Loccufier, W. De Waele, Numerical framework for fatigue lifetime prediction of complex welded structures, Frattura ed Integrita Strutturale 14 (51) (2020) 552–566. doi:10.3221/IGF-ESIS.51.42.

Declaration of interests

☒ The authors declare that they have no known competing financial interests or personal relationships that could have appeared to influence the work reported in this paper.

☐The authors declare the following financial interests/personal relationships which may be considered as potential competing interests:

Kris Hectors: Conceptualization, Methodology, Software, Validation, Investigation, Writing - Original Draft, Visualization **Wim De Waele:** Conceptualization, Methodology, Validation, Writing – Review and Editing, Supervision, Funding acquisition